Proceedings of the 13th International Symposium on Experimental Computational Aerothermodynamics of Internal Flows
7–11 May 2017, Okinawa, Japan

ISAIF13-S-0056

Experimental validation of the continuous evolution of flow topology from compressor mode to highly loaded windmill of low-speed axial machines

Aurélie ORTOLAN[1,2], Suk-Kee COURTY-AUDREN[1], Xavier CARBONNEAU[1], Nicolas BINDER[1], and Florent CHALLAS[2]

1 ISAE-SUPAERO
Avenue Edouard Belin, 10, 31400, Toulouse, France,
aurelie.ortolan@isae.fr, +33561338774

2 SAFRAN Technofan
Place Marcel Dassault, 10, 31700, Blagnac, France

Abstract

In aeronautics, onboard axial fans, only used on the ground to cool heat exchangers, can be regarded as potential electrical generation devices when operating at freewindmill in flight. In this case, the appropriate windmilling configuration is the load-controlled one, from which energy recovery is possible. This paper presents a detailed experimental analysis, on a conventional axial compressor, of the continuous local topology evolution on both rotor and stator rows from compressor mode to highly loaded windmill. The objective is to deepen the understanding of windmilling flows and validate experimentally numerical results obtained on a previous paper from the present authors. In this latter, the innovative concept of a dual machine, meant to reach good performances in both compressor and turbine modes, was presented and numerically validated. The present paper experimentally confirms the relevance of the new design.

Keywords: Windmilling, energy recovery, continuous topology evolution, experimental validation.

Introduction

Since a few years, many studies have been carried out on the freewheeling operation of turbofans in situation of engine flame-out to assess their relight capabilities. In this windmilling configuration, the work exchange through the rotor is generally neglected. The trend towards more electric aircrafts has increased the need for onboard electrical power. This gives another dimension to windmilling studies. As new electrical sources must be found, windmill is regarded as a potential energy generating mode. Currently, onboard axial fans are dedicated to the cooling of heat exchangers on the ground. In flight, they are of no use and windmill freely due to the massflow created through the ram air (Fig. 1). Such machines are dead weight during cruise and can be exploited to generate electricity by applying a resistive torque on the shaft to slow down the free rotation of the rotor. This operating regime is called load-controlled windmill and is located between locked rotor configuration and freewindmill.

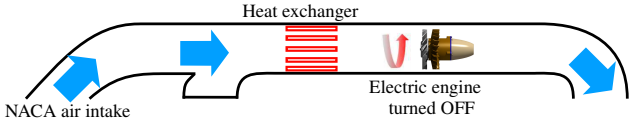

Figure 1 Configuration in flight conditions.

The first study dealing with the complete global performances of an axial compressor is attributed to Turner and Sparkes [1] who first introduced four quadrant diagrams. In their paper, the presented temperature rise to flow coefficient diagram showed the continuity of the machine characteristics when switching from the first (compressor) to the fourth quadrant (load controlled windmill). However, no local analysis is given. A more recent work [2] presents radial distributions of the loading coefficient and velocity components for only three flow coefficients in the fourth quadrant. Seemingly, the first operating point corresponds to the stirrer mode ($\Delta h_i > 0$, $\Delta P < 0$), the second one to freewheeling mode ($\Delta h_i \approx 0$, $\Delta P < 0$) and the third one to turbine operation ($\Delta h_i < 0$, $\Delta P < 0$). This study does not cover the highly loaded windmilling regime. However, in Goto's paper [3], a pressure-rise to flow coefficient map is given from compressor to sligthly loaded windmill with a discretization of about $\Delta\phi = 0.2$. Courty-Audren in a recent work [4] presents a numerical study of secondary flow evolution from compressor to load-controlled windmill. Finally, Binder [5] proposed an analytical approach which underlines the continuity of the loading-to-flow coefficient characteristics [6, 7]. This model also explains the origin of the dual functioning of the rotor (compressor/turbine cohabitation on the blade) over a given oper-

ating range around the freewindmilling condition (switch zone) [8, 9]. For a better understanding, velocity diagrams in compressor, freewindmill and load-controlled windmill are presented in Fig. 2.

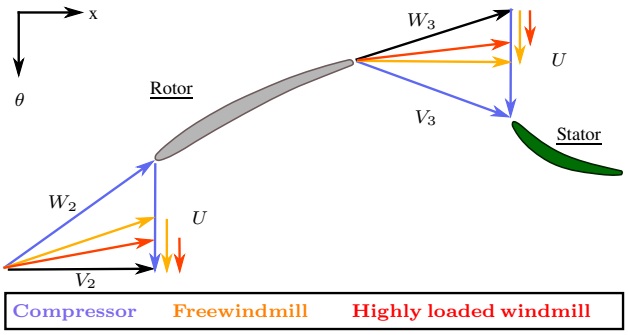

Figure 2 Velocity diagrams at compressor and windmill.

The present paper intends to validate the continuity of the flow properties when switching from compressor operation to highly loaded windmill on a conventional axial fan. Both global and local performances are addressed. On a previous work of the present author [9], this fan and a dual machine, meant to reach high performances in both compressor and load-controlled windmill, were numerically investigated. The present paper also aims at validating the previous numerical results, in particular the relevance of the optimized design.

The main topics investigated in this paper are:

- the continuity of global performances, especially regarding the $(\hat{\psi}, \hat{\phi})$ and $(\hat{\phi}, \eta)$ characteristics;
- the continuity of the local flow topology up to highly loaded windmill at rotor inlet/outlet and stator outlet;
- the validation of the dual machine concept from tests.

Test cases

The machines studied are low-speed axial fans composed of a single rotor-stator stage. In Tab. 1, properties of the conventional compressor (Fan 1) and dual machine (Fan 2) are presented but for confidential reasons few data can be published. Fan 2 was designed using a nonconventional procedure. The rotor was entirely modified to be able to efficiently extract or give work in both compressor and turbine operations. As reported many times in the literature [8–11], classical fans are characterized by massive separations in the stator where most of the losses occur at windmill. Consequently, a variable camber one was imagined to adapt the leading edge to the local direction of the flow and prevent massive separations on the blade suction side.

Table 1 Machines properties

	Fan 1	Fan 2
Diameter (mm)	≤ 200	≤ 200
Rotor blades	17	13
Stator blades	23	27
Design rotational speed (rpm)	≈ 12000	≈ 20000

In this paper, the $(\hat{\psi}, \hat{\phi})$ formalism is used to give a unique representation of the global performances for both compressor and windmilling modes. The relevance of such a model for the study of far-off designs cases has been demonstrated by the literature [1, 5]. In addition, as several machines are studied, another useful parameter has to be introduced: the reduced flow coefficient $\hat{\phi}^*$, which is equal to the flow coefficient of a given operating point divided by its value at freewindmill. This enables to compare the global performances at the same incursion level in both compressor and turbine operations. These parameters are expressed as follows:

$$\begin{cases} \hat{\psi} = \dfrac{\Delta h_{i23}}{\hat{U}^2} & (1) \\ \hat{\phi} = \dfrac{V_{x2}}{\hat{U}} & (2) \\ \hat{\phi}^* = \dfrac{\hat{\phi}}{\hat{\phi}_P} & (3) \\ \hat{r} = \sqrt{\dfrac{r_{shroud}^2 + r_{hub}^2}{2}} & (4) \\ \hat{U} = \omega \hat{r} & (5) \end{cases}$$

Experimental Facility

Experiments were carried out in the Department of Aerodynamics, Energetics and Propulsion (DAEP) of ISAE-SUPAERO. A test facility was specifically designed to study the windmilling operation of low-dimension axial fans. An illustration of the test rig is visible on Fig. 3.

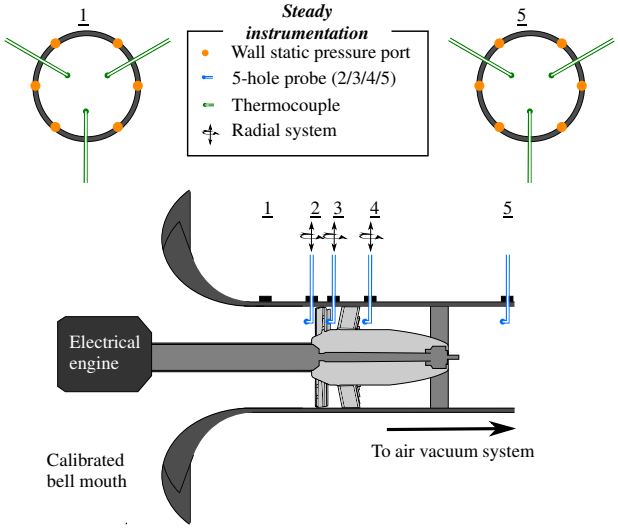

Figure 3 Illustration of the DAEP windmilling test facility.

Flow generation is independently ensured by either the asynchronous electrical engine (compressor mode) or the air vacuum system by suction (freewndmilling mode). The combination of these two systems enables to work in load-controlled windmill by applying a given torque on the shaft. In addition, the instrumented part, including the fan, can be inverted to change the flow direction. This means

that every operating point from compressor surge to locked rotor configuration is reachable. During tests, the rotational speed and torque are controlled and measured thanks to a torque meter (Magtrol TM 306) coupled with the electrical engine. The latter has been deported far from the test section to protect the measurement from electromagnetic disturbance.

Regarding the steady instrumentation, the test rig is composed of five measurement planes located after a calibrated bell mouth used to assess the massflow through the test section. Planes 1 and 5 correspond to the general inlet and outlet of the instrumented part. They are used to get the global performances of the machines thanks to 3 thermocouples (Type K, basic accuracy 1 °K) equally spaced in the azimuthal direction and a 6-hole Kent chamber connected to a differential sensor (Rosemount, $0/100$mbars, basic accuracy 0.15% FS). This enables to measure the mean total temperature and the mean static pressure. The outlet is also equipped with a fixed five-hole probe that gives the total pressure (Keller, $-150/+100$mbars, basic accuracy 0.047% FS). Local characterizations are obtained at rotor inlet (Plane 2), rotor outlet (Plane 3) and stator outlet (Plane 4), thanks to directional five-hole probes (Keller, $-150/+100$mbars, basic accuracy 0.047% FS, Rosemount $-50/50$mbars, basic accuracy 0.15% FS). The radial probing of velocity field and pressure is conducted from hub to shroud through around 30 positions. Data acquisition is achieved by a composite NI cDAQ-9172 device connected to 3 kind of NI modules that are used for current (NI 9215), voltage (NI 9203) and temperature (NI 9211) recordings. The measurements were acquired on 5000 samples with a sampling frequency of 20kHz.

During the experimental campaign, operating points from compressor surge ($\hat{\phi}^* = 0.3$) to highly loaded windmill ($\hat{\phi}^* = 3$) were explored with global steady instrumentation every $\Delta\hat{\phi}^* = 0.05$. Local distributions were obtained for 9 selected operating points : $\hat{\phi}^* = 0.6$, $\hat{\phi}^* = 0.66$ (compressor peak efficiency point), $\hat{\phi}^* = 0.8$, $\hat{\phi}^* = 1$ (freewindmill), $\hat{\phi}^* = 1.2$, $\hat{\phi}^* = 1.5$ (near turbine peak efficiency point), $\hat{\phi}^* = 2$, $\hat{\phi}^* = 2.5$, $\hat{\phi}^* = 3$ (highly loaded windmill).

Global performances

Figure 4 shows the global performances of the conventional fan in the loading to reduced flow coefficient diagram. The reduction of the flow coefficient by its value at freewindmill makes the line intersect at $\hat{\phi}^* = 1$ (freewindmill). Three modes are observed: compressor, stirrer and load-controlled windmill. The stirrer mode is generally out of reach for classical test benches. However, with the present facility, the combination of the vacuum system and electrical engine makes stirrer operation possible. For each behaviour, a linear fit is plotted underlining an increasing negative slope. The analytical model proposed by Binder [5] relates the slope of the $(\hat{\phi}^*, \hat{\psi})$ characteristics to two main parameters: the relative flow angle at rotor outlet and the mean quadratic radius. The observed slope variations are believed to come from small changes in flow angle. As stated in [12], flow deviation depends on blade loading (Kutta-Joukowski condition at the trailing edge). For conventional operating range, the blade loading remains almost the same for a given fan. In the present case, suction and pressure sides are inverted from compressor to loaded windmill, as observed in [4]. This is likely to be responsible for small changes in the deviation which entails a discontinuity in the slope. Such a behaviour has already been observed in the literature for some geometries [13].

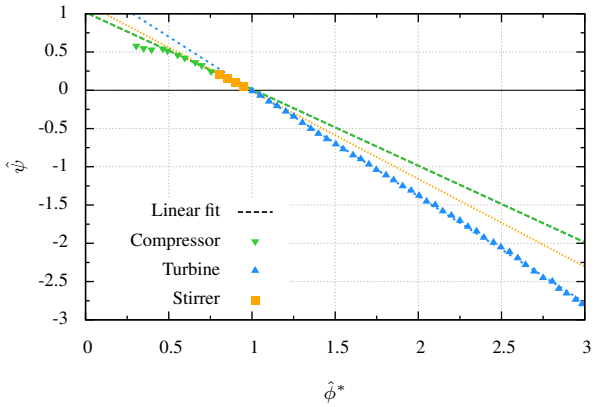

Figure 4 Loading to reduced flow coefficient diagram.

Figure 5 shows the total-to-total efficiency evolution. Classical definitions are used for compressor and turbine modes. The compressor efficiency definition is used for the stirrer mode. In this latter, two points are characterized by very negative values of efficiency. For readability purposes, their location are indicated with arrows. This figure illustrates the poor efficiency recorded in windmilling mode for the conventional fan. It is four times lower than that of the compressor operation. This observation is in agreement with the literature which reports maximum turbine efficiencies of about 0.2. This figure also confirms the diverging behaviour of the efficiency in the stirrer region previously reported by Gill [2].

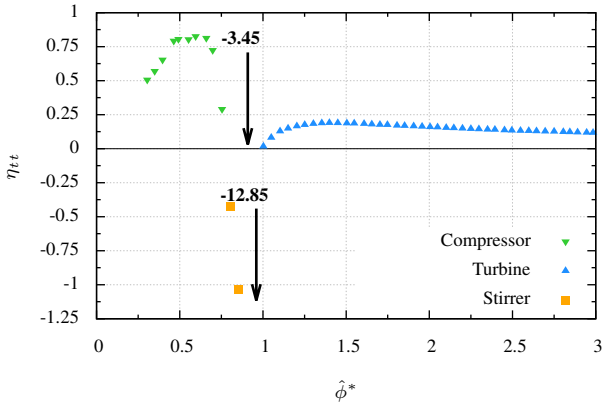

Figure 5 Efficiency to reduced flow coefficient diagram.

Rotor local topology evolution

Evolutions of relative incidence at rotor inlet are depicted in Fig. 6. As visible on the graph, the increase in reduced flow coefficient is directly reflected in a decrease in incidence towards negative values. This is expected since, for purely axial incoming flow, the simple relationship between relative flow angle at rotor inlet and the flow coefficient can be derived from velocity triangles:

$$\beta_2 = \frac{\pi}{2} - arctan(\phi) \tag{6}$$

For the smallest flow coefficient, the incidence is nearly constant along the span and equals to zero which means that every blade section operates near its nominal incidence. The increase in flow coefficient is associated with a distortion from hub to tip generally smaller than 5°. Almost linear distributions are reported, characterized by more negative values near the hub. This may be caused by the blockage of the upper blade sections reported in the literature which implies a local increase in axial velocity near the hub, as shown in the following paragraph.

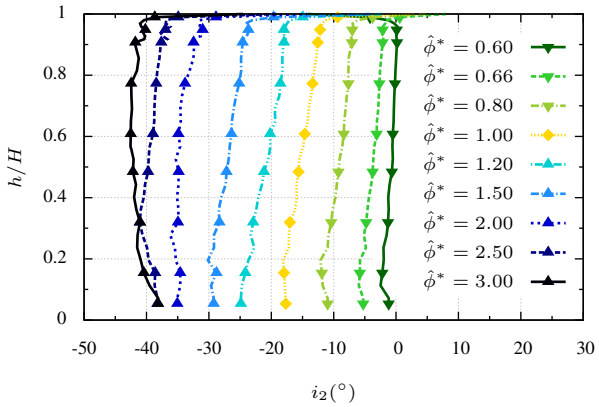

Figure 6 Incidence at rotor inlet.

Figure 7 presents the distributions of adimensionalized axial velocity at rotor outlet. In this figure, the increase of flow coefficient leads to a growing vein blockage in the tip region. As a consequence, significant radial gradient

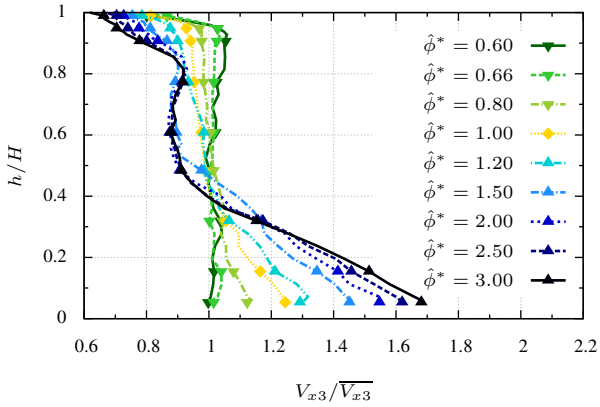

Figure 7 Adimensionalized axial velocity at rotor outlet.

of axial velocity is reported in highly loaded windmilling. In addition, radial distributions of the three highest flow coefficient are almost identical from midspan to 80% of the vein which suggest that separation does not evolve beyond $\hat{\phi}^* = 1.5$. On the contrary, a continuous decrease of axial velocity is observed in tip region which is related to the tip leakage flow. Finally, a continuous increase of velocity in the first half of the blade is reported.

Figure 8 shows the evolution of the rotor outlet deviation from compressor to highly loaded windmill. As can be seen, the distribution becomes more distorted while going towards turbine operation. Gunn [10] also observed that the deviation at feewindmill slightly differs from that of the compressor mode along the whole span. For the four greater flow coefficients, a change in the distribution shapes is reported. The deviation profiles are bilinear with a slope change located between 30% and 50% of the span. This height matches the radial location of the massive flow separation on the blade [9].

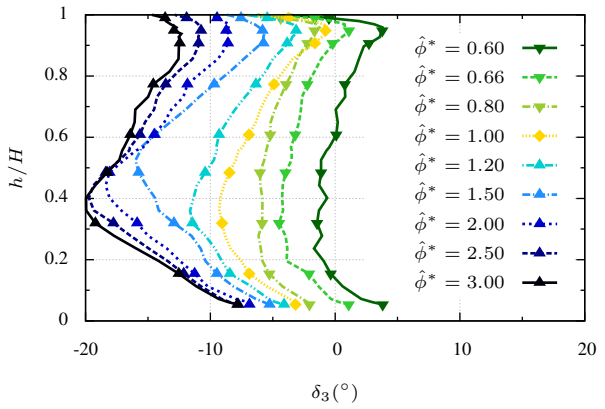

Figure 8 Deviation at rotor outlet.

Radial distributions of loading coefficient are depicted in Fig. 9. The observed profiles are linear from compressor to slightly loaded windmill, as beyond $\hat{\phi}^* = 2$, the profile is distorted underlining a significant decrease in work coefficient near midspan. These distorsions are related to the work distribution shapes since U^2 always evoles as a quadratic function of the radius. As the experimental total enthalpy variations are calculated from the tangential velocity changes between rotor inlet and outlet, the origin of this deficit is related to the radial distribution of the deflection. In addition, the switch zone, located at the boundary between compressor and load windmill, should be visible experimentally. For the recall, this region corresponds to an operating range for which a coexistence of compressor (near the hub) and turbine modes (near the shroud) is recorded on the blade. For Fan 1, its width is numerically assessed at a value of about 0.14 in terms of reduced flow coefficient variations [9]. On this figure, as the minimum value of $\Delta\hat{\phi}^*$ is 0.2, only the operating point $\hat{\phi}^* = 1$ is part of the switch zone. It can be seen that the first 10% of the blade span near the hub works as a compressor ($\psi > 0$) where the remaining blade span works as a tur-

bine ($\psi < 0$). Actually, a more detailed discretization near freewindmill would have been too costly since there is no discontinuity in this region.

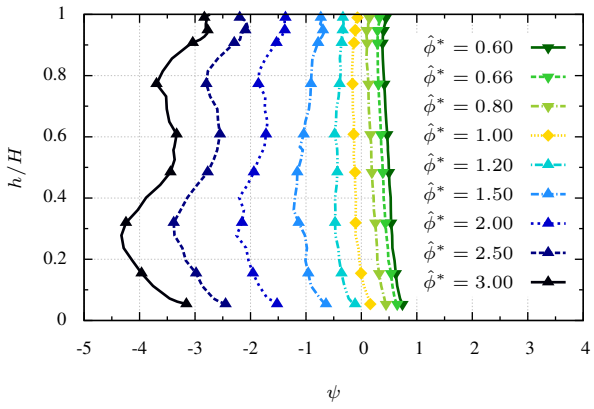

Figure 9 Rotor loading coefficient.

Figure 10 presents the radial distributions of the losses through the rotor. The work contribution to the total pressure variation has been removed, under the incompressible assumption. Its evolution with the reduced flow coefficient highlights a strong change of topology for the most loaded cases. The distorted distribution of the losses at highly loaded windmill corresponds to the signature of the rotor separation at mispan and the presence of a strong tip leakage flow near the shroud.

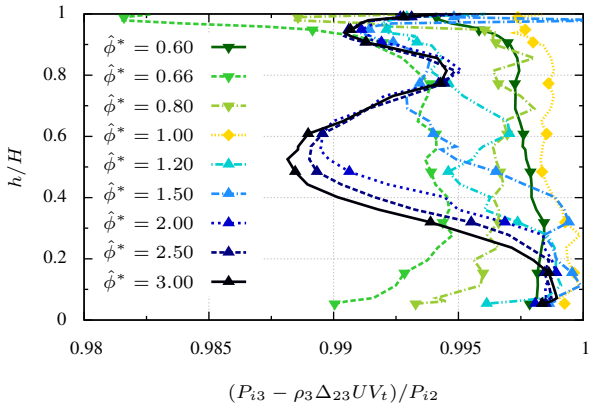

Figure 10 Loading coefficient.

Stator local topology evolution

In this section, the continuity of topology in the stator is investigated. Evolutions of incidence with operating points are presented in Fig. 11 for Fan 1. This figure underlines the highly negative values obtained at windmill. The stacking of this blade row is constant. Consequently, the observed change in incidence from hub to tip can be solely imputed to absolute flow angle distributions. Nearly constant along the span in compressor operation, the distribution of incidence progressively becomes linear at slightly loaded windmill. At highly loaded windmill ($\hat{\phi}^* = 2$ to 3), a slope break is observed near 30% of the blade span, which corresponds to the beginning of the massive separation on the rotor blade. From hub to shroud, almost 40° degrees of variation are reported. The velocity deficit in the separation region from 30% of the blade span is expected to reduce a little the incidence as suggested in [11].

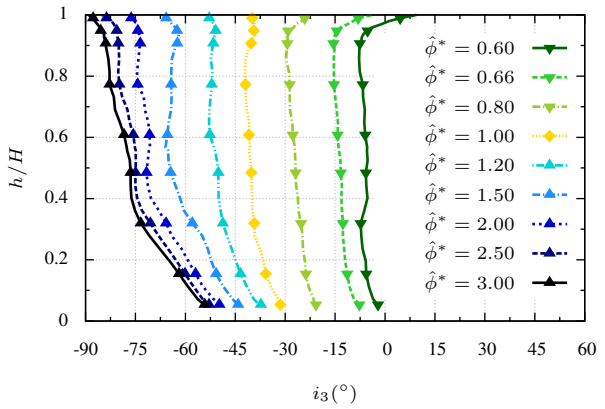

Figure 11 Incidence at stator inlet.

Figure 12 presents the distributions of reduced axial velocity at stator outlet. As observed at rotor outlet, axial velocity profiles at stator outlet are characterized by high velocities located near the shroud for compressor operating points and near the hub in load windmill. These distributions are due to the displacement of the blockage area from compressor to turbine operation. In compressor mode, no separation is generally reported as blade profiles undergo limited incidences. The outlet metal angle of the stator is constant so that the distribution of absolute tangential velocity can be assumed uniform. The simplified radial equilibrium applied at stator outlet leads to an increasing axial velocity from hub to tip if entropy variation with the radius are neglected. In load windmill, increasing massive separations are reported near the shroud of stator rows which causes a increased blockage in the upper sections of the vein. The axial velocity consequently increases in the hub region.

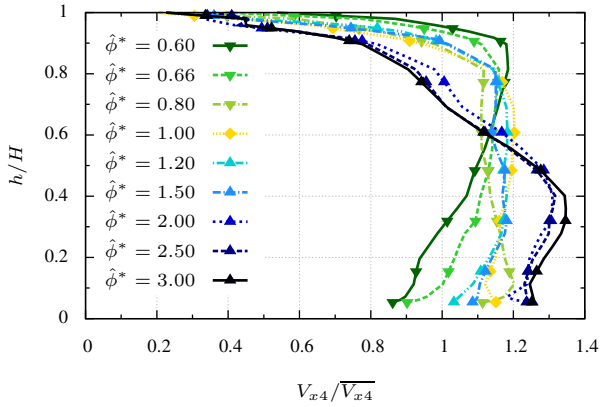

Figure 12 Adimensionalized axial velocity at stator outlet.

An insight of the stator losses is visible on Fig. 13 by means of the total pressure ratio. The very low amount recorded in compressor mode show that the stator is well-suited to this mode. From freewindmill, the losses begin to increase significantly. A specific pattern appears for the three most loaded operating points. For these cases, the total pressure drop in both rotor and stator massive separation regions is certainly responsible of this result.

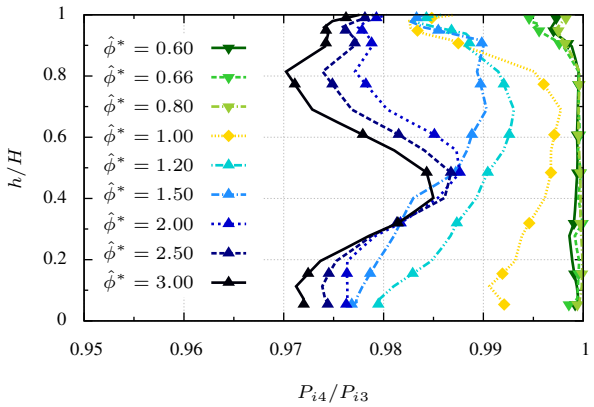

Figure 13 Loading coefficient.

Experimental validation of the dual machine

The objective of this last section is to check experimentally the promising performances recorded numerically for the dual machine in both compressor and turbine operations on a previous paper [9].

The $(\hat{\psi}, \hat{\phi}^*)$ characteristic is given on Fig. 14. As for Fan 1, three operating modes are observed on Fan 2. Likewise, a change in slope is observed but appears for higher values of reduced flow coefficient than for Fan 1 (around $\hat{\phi}^* = 2$). This can be imputed to the new design procedure which enables to delay the appearance of critical negative incidences, in particular by a reducing camber.

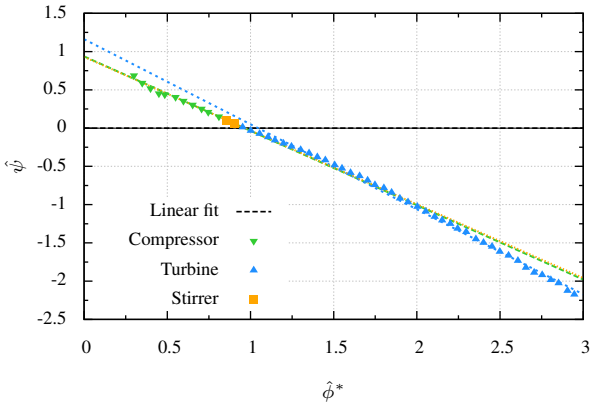

Figure 14 Loading to reduced flow coefficient diagram.

The total-to-total efficiency, plotted in Fig. 15 for Fan 2. It highlights the good performances of the dual machine in windmilling operation. The turbine maximum efficiency is

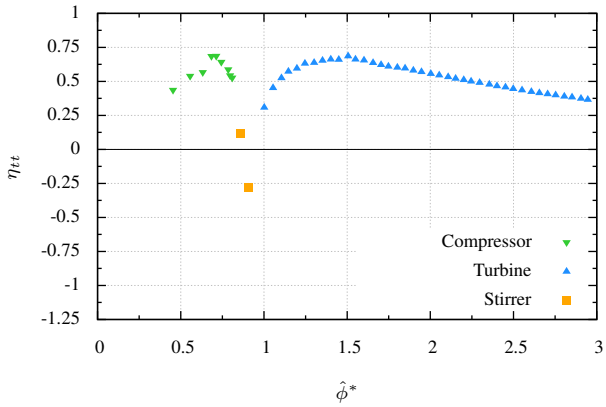

Figure 15 Efficiency to reduced flow coefficient diagram.

of the same order of magnitude of the compressor one. The experiments confirms the numerical trend regarding the dual machine high performances. This figure also shows a reduced operability in compressor mode which operating range is around $\Delta\hat{\phi}^* = 0.25$.

The local evolution of the loading coefficient is presented in Fig. 16. As can be seen, the work done at freewindmill is nearly zero along the span, as expected from the design procedure which intends to suppress the mixed local behaviour, thanks to a constant work distribution. Consequently, the compressor and turbine operations are completely separated, underlining the relevance of this design to properly operate in antagonist modes.

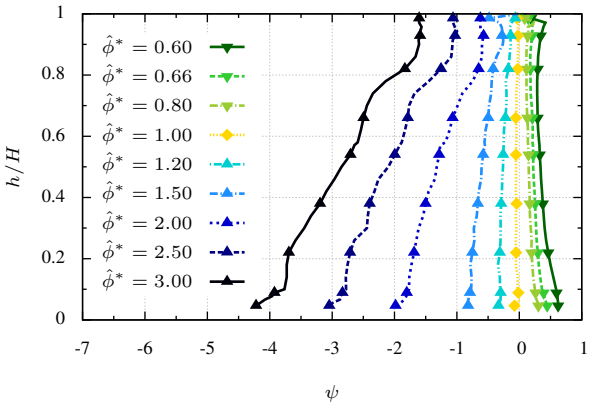

Figure 16 Rotor loading coefficient.

Conclusions

In this study the evolution of flow properties from compressor to turbine mode is investigated on axial fans. The novelty of the paper is the investigation of very highly loaded windmill mode. Local and global flow properties of such operating points differ significantly from freewindmilling ones. In particular, specific deviation rules in situation of massive separation must be derived to properly predict flow deflection in early design steps. The most important results of the paper are summarized below:

- Compressor and turbine ($\hat{\phi}^*$, $\hat{\psi}$) characteristics are

slightly different: a break of the slope is reported;
- Local topology evolve continuously from compressor to moderated loaded windmill ($\hat{\phi}^* < 2$)
- Local topology is significantly different in highly loaded windmilling (starting from $\hat{\phi}^* = 2$)
- Experimental loss estimation confirms that most of the losses occur in the stator row
- The innovative design high efficiencies in compressor and turbine mode is confirmed.

Acknowledgements

The authors would like to thank the CORAC GENOME project, in the scope of which this study was performed. Its objective is to optimize the power management in more electric aircrafts. This program was created on the government initiative to harmonize the research efforts in aeronautics. Likewise, the authors would like to express their deep gratitude to the technical staff in charge of the test facility because, without their constant investment, the experimental data presented in this paper would not have been obtained in time.

References

[1] Turner, R. C. and Sparkes, D. W., (1963), Complete characteristics for a single stage axial flow fan, In Proceedings of the Institution of Mechanical Engineers, Conference Proceedings 1963, Vol. 178.

[2] Gill, A., (2011), Four quadrant axial flow compressor performance, PhdThesis, Stellenbosch university.

[3] Goto, T., Kato, D., Ohta, Y. and Outa, E., (2014), Unsteady flow structure in an axial compressor at windmill, ASME Turbo Expo, June 16-20, Düsseldorf, Germany, GT2014-25609.

[4] Courty-Audren, S.-K., Ortolan, A., Carbonneau, X., Binder, N. and Challas, F., (2017), Numerical analysis of secondary flow topologies of low-speed axial fans from compressor to load-controlled windmill. In Proceedings of the 12th European Conference on Turbomachinery, April 3-7, Stockholm, Sweden, ETC2017-323 (submitted).

[5] Binder, N., Courty-Audren, S.-K., Duplaa, S., Dufour, G. and Carbonneau, X., (2015), Theoretical analysis of the aerodynamics of low-speed fans in free and load-controlled windmilling operation, ASME Journal of Turbomachinery, 137(10), pp. 101001-12.

[6] Courty-Audren, S.-K., Carbonneau, X., Binder, N. and Challas, F., (2013), Potential of power recovery of an axial fan in windmilling operation, In Proceedings of the 10th European Conference on Turbomachinery, April, Lappeenranta, Finland. ETC2013-094.

[7] Ortolan, A., Courty-Audren, S.-K., Carbonneau, X., Binder, N. and Challas, F., (2017), Experimental and numerical flow analysis of low-speed fans at highly loaded windilling conditions, ASME Journal of Turbomachinery. 139(7), pp. 071009-8.

[8] Prasad, D., Lord, W. K., (2010), Internal losses and flow behavior of a turbofan stage at windmill, ASME Journal of Turbomachinery, Vol. 132, March, pp. 031007 (10 pages).

[9] Ortolan, A., Carbonneau, X., Binder, N., Challas, F. and Meauze, G., (2015), Innovative fan design for both high compressor and windmilling performance, In Proceedings of the 12th International Symposium on Experimental and Computational Aerothermodynamics of Internal Flows, July 13-16, Lerici, Italy, ISAIF12-068.

[10] Gunn, E. J. and Hall, C. A., (2015), Loss and deviation in windmilling fans. In Proceedings of the 11th European Conference on Turbomachinery, March 23-27, Madrid, Spain, ETC2015-061.

[11] Dufour, G., García Rosa, N. and Duplaa S., (2015), Validation and flow structure analysis in a turbofan stage at windmill, Journal of Power and Energy, 229(6), pp. 571-583.

[12] Cumpsty, N. A., (2004), Compressor aerodynamics, Krieger.

[13] McKenzie, A. B., (1997), Axial flow fans and compressor - Aerodynamic design and performance, Cranfield series on turbomachinery technology.